Journal of Biomechanics 164 (2024) 111951

Contents lists available at ScienceDirect

Journal of Biomechanics

journal homepage: www.elsevier.com/locate/jbiomech

Assessment of a fully-parametric thoraco-lumbar spine model generator with articulated ribcage

Emilia Bellina [a,b], Maria Elvira Laurino [a], Alice Perego [a], Alice Pezzinga [a], Linda Carpenedo [a], Davide Ninarello [a], Luigi La Barbera [a,c,*]

[a] Laboratory of Biological Structure Mechanics, Department of Chemistry, Materials and Chemical Engineering "Giulio Natta", Politecnico di Milano, Milan, Italy
[b] IRCCS Humanitas Research Hospital, Milan, Italy
[c] IRCCS Galeazzi-Sant'Ambrogio Hospital, Milan, Italy

ARTICLE INFO

Keywords:
Spine
Biomechanics
Parametric Model
Computer Aided Design (CAD)
Finite Element Model (FEM)

ABSTRACT

The present paper describes a novel user-friendly fully-parametric thoraco-lumbar spine CAD model generator including the ribcage, based on 22 independent parameters (1 posterior vertebral body height per vertebra + 4 sagittal alignment parameters, namely pelvic incidence, sacral slope, L1-L5 lumbar lordosis, and T1-T12 thoracic kyphosis). Reliable third-order polynomial regression equations were implemented in Solidworks to analytically calculate 56 morphological dependent parameters and to automatically generate the spine CAD model based on primitive geometrical features. A standard spine CAD model, representing the case-study of an average healthy adult, was then created and positively assessed in terms of spinal anatomy, ribcage morphology, and sagittal profile.

The immediate translation from CAD to FEM for relevant biomechanical analyses was successfully demonstrated, first, importing the CAD model into Abaqus, and then, iteratively calibrating the constitutive parameters of one lumbar and three thoracic FSUs, with particular interest on the hyperelastic material properties of the IVD, and the spinal and costo-vertebral ligaments.

The credibility of the resulting lumbo-sacral and thoracic spine FEM with/without ribcage were assessed and validated throughout comparison with extensive *in vitro* and *in vivo* data both in terms of kinematics (range of motion) and dynamics (intradiscal pressure) either collected under pure bending moments and complex loading conditions (bending moments + axial compressive force).

1. Introduction

Spine models are a valuable tool to better elucidate the basic biomechanics underlying specific patho-physiological mechanism, as well as to support the clinical/surgical decision-making process.

Depending on the specific research objectives, a variety of modelling approaches could be justified and adopted. For instance, any spine expert should decide for one among alternative options: patient- vs. cohort- vs. population-specific approach, anatomical fidelity vs. simplified geometrical features, few vs. many functional spinal units (FSUs), inclusion of the anterior column (i.e. vertebrae, intervertebral disc) vs. anterior + posterior (lamina, facet joints, spinal processes) columns, inclusion of osteo-ligamentous passive vs. active muscular structures, linear vs. non-linear mechanical properties, homo- vs. hetero-geneous material properties, simplified (i.e. pure bending moment) vs. complex (follower load + bending moment) vs. realistic (muscle forces + gravity loads) loadings.

Many researchers have developed and validated excellent spine models often focusing on a limited spine segment including few FSUs (typically L1-S1), broadly respecting spine anatomy, assuming heterogeneous non-linear material properties, and they performed reasonable predictions under simplified and complex loadings either predicting kinematics, dynamics and the specific stress/strain on a given spinal structure (Dreischarf et al., 2014, ElBojairami et al., 2020, Schmidt et al., 2012, Ottardi et al., 2016, Rohlmann et al., 2009). A completely different approach consists in developing musculoskeletal multi-body models of the thoraco-lumbar spine (typically T1-S1), sometimes including the ribcage, where bony parts are assumed as rigid bodies, the intervertebral disc (IVD) is reduced to a joint with limited degrees-of-freedom, and the posterior column is neglected (Ignasiak et al., 2016,

* Corresponding author.
E-mail address: luigi.labarbera@polimi.it (L. La Barbera).

https://doi.org/10.1016/j.jbiomech.2024.111951
Accepted 11 January 2024
Available online 20 January 2024

Bruno et al., 2015). Such an approach allows describing the complex muscular activation pattern, but it only provides generalized insights on spine kinematics and dynamics.

Current research is pushing to extend the validity of the results achieved using individualized spine models. In several cases, it is unclear whether the model takes inspiration from one specific subject, or it features average morphological characteristics to make it representative of one specific cohort, or maybe, an entire population.

Several pipelines have been proposed to generate spine models based on reconstruction of clinical images, or based on statistical approaches (i.e. principal component analysis), but they are time consuming, computationally expensive, and limited by the availability of extensive, reliable and complete clinical databases (Wang et al., 2016, Park et al., 2017, Lavecchia et al., 2018, Laville et al., 2009, Bassani et al., 2017). Parametric spine modelling is an alternative option requiring limited clinical information, allowing to quickly generate spine models easily scalable to create a wide range of *in silico* virtual cohorts with controlled features (Nikkhoo et al., 2020, Niemeyer et al., 2012, Bashkuev et al., 2018, Lavaste et al., 1992; Maurel et al., 1997).

Niemeyer et al. (2012) and Bashkuev et al. (2018) proposed two similar finite element model generators requiring 40 inputs to generate a single lumbar (i.e. L4-L5 FSU, including 17 parameters for vertebra plus additional 6 for intervertebral region and spinal processes). Lavaste et al. (1992) required instead 6 inputs parameters per vertebra, to be identified on antero-posterior and lateral X-ray clinical images. Recently, Nikkhoo et al. (2020) proposed a parametric lumbar spine model based on few parameters (5 for VB, 6 for FJs, 4 for the posterior spinous process, 2 for the lateral spinous process and 4 for foramen and lamina), however, it only focused on the lumbar spine segment (i.e. L1-S1) and assumed mechanical properties from literature.

Despite several authors generated thoracolumbar spine models with/without the ribcage based on reconstructed clinical images, no purely parametric geometric spine model of the entire thoracic segment alone, nor including the ribcage is available to date. Some study proposed a parametric ribcage geometric model accounting for variations among the adult population based on statistical analyses and linear regression. Wang et al., (2016) mesh morphed a template model on clinical images from 101 patients and applied generalized procrustes and principal component analysis) to derive ribcage model parameters (Wang et al., 2016). Holcombe et al., (2016) parametrized the ribs' shape of 100 adults only using 6 parameters to approximate each rib with logarithmic spirals (Holcombe et al., 2016).

The present paper aimed at: i) developing a fully-parametric thoracolumbar spine CAD model generator comprehensive of the ribcage based on few independent parameters to describe a variety of sagittal profiles; ii) assessing its credibility throughout the comparison of a generated standard model representing the case-study of a healthy male adult with extensive *in vitro* and *in vivo* data both in terms of morphology, kinematics and dynamics both collected under simplified and complex loading conditions.

2. Methods

2.1. Parametric thoraco-lumbar spine CAD model generator

Regression analyses: fifty-six dependent parameters describing the morphological features of each vertebral body (VB), lamina or vertebral arch (VA), spinal process, facet joint (FJ), intervertebral disk (IVD), ribs and sternum were best-fitted using third-order polynomial analytical equations as a function of VBHP (vertebral body posterior height), assumed as the only independent parameter for each vertebra (Supplementary Material–Table 1). A total of seven dependent parameters were used for the anterior column (six for each VB, one for the IVD) (Panjabi et al., 1992, Panjabi et al., 1991; Panjabi et al., 1993, Kunkel et al., 2011), ten for the posterior column (i.e. VA) (Panjabi et al., 1992, Panjabi et al., 1991, Abuzayed et al., 2010, Kaur et al., 2016, Shaw et al., 2015, Cui et al., 2015), eleven for the posterior column (i.e. FJ) both for the thoracic and lumbar vertebrae (Panjabi et al.,1993), fourteen for each rib, which were described as planar logarithmic spirals, plus three for the sternum (Holcombe et al., 2017, Mohr et al., 2007). For each spinal level, mean anatomical data for every parameter were taken from literature, keeping a consistent definition (Supplementary Material–Table 1). The coefficient of determination (R^2) and the Root Mean Square Error (RMSE) quantified the goodness-of-fit for each generated analytical equation.

Parametric CAD drawing: for each of eighteen vertebrae a corresponding part was created in SOLIDWORKS 2021 (SolidWorks Corporation, Waltham, MA, USA), where vertebral morphology was reduced to simple primitives features and equations were automatically implemented. VBs, pedicles and facets were assumed as extruded ellipses, while the lamina and spinal processes through extruded prisms with rectangular or elliptical section. Each IVD was extruded on the corresponding caudal VB; then divided into annulus fibrosus (AF) and nucleus pulposus (NP), whose position and proportion derived from (Kapandji et al., 2012). The ribs were drawn using sweep function to extrude an elliptical section in the same part of the corresponding vertebra, defining a new local plane and assuming a uniform cortical thickness of 0.76 mm (Mohr et al., 2007). The sternum, defined as manubrium, body, and xiphoid process, was extruded on a local plane originating at the midpoint of the second rib, assuming a uniform thickness of 8.1 mm (Xiu et al., 2012). The costal cartilage was drawn extruding the elliptical section along a three-point arc using loft function which reached seven sternal notches (Holcombe et al., 2017). Ligaments were designed directly on the resulting assembled CAD model, identifying convenient surfaces.

Sagittal alignment: PI (pelvic incidence), PTH (pelvic thickness), SS (sacral slope), L1-S1 LL (lumbar lordosis), and T1-T12 TK (thoracic kyphosis) were introduced as additional (independent) sagittal alignment parameters to assemble each cranial vertebra on top of the corresponding caudal one and to achieve the final spinal profile.

2.2. Case study

Generation of a Standard CAD model: to demonstrate the feasibility of creating a quantitatively self-consistent CAD model ready for computational analyses, a standard CAD model representing a healthy male adult (age 46.3 years, height 167.8 cm, weight 67.8 kg) was generated assuming average measurements for each VBHPs (Panjabi et al., 1992). Consistent PI, PTH, SS, LL, and TK were set equal to 45.9° (Vrtovec et al., 2013), 104.9 mm (Vrtovec et al., 2012), 38° (Pesenti et al., 2018), 58° (Pesenti et al., 2018), and 45° (Harrison et al., 2001). A percentage distribution of TK and LL at each functional spinal unit was assumed (Pesenti et al., 2018; Harrison et al., 2001). The standard CAD model was finally generated (Fig. 1).

Assessment and validation: sagittal alignment parameters of the standard CAD model were compared with *in vivo* clinical data (Vrtovec et al., 2013, Vrtovec et al., 2012, Pesenti et al., 2018, Harrison et al., 2001, Fasser et al., 2021, Bruno et al., 2015). Ribs' morphology was compared in terms of chord and arc lengths as measured *ex vivo* (Dansereau and Stokes, 1988), while sternum position and orientation relative to the thoracic segment were compared with *in vivo* data (Burgos et al., 2021).

2.3. Case study: Calibration of lumbar and thoracic FSUs FEMs

To demonstrate the suitability of the standard CAD model to generate detailed FE biomechanical models, each part was sequentially imported and meshed in Abaqus 2022 (Dassault Systemes, Simulia, Johnston, RI, USA).

Orthotropic linear elastic properties were assigned to the trabecular and cortical VB parts, while assuming isotropic linear elastic for VA and cartilages (Supplementary Material–Tables 2, 3). Hyperelastic

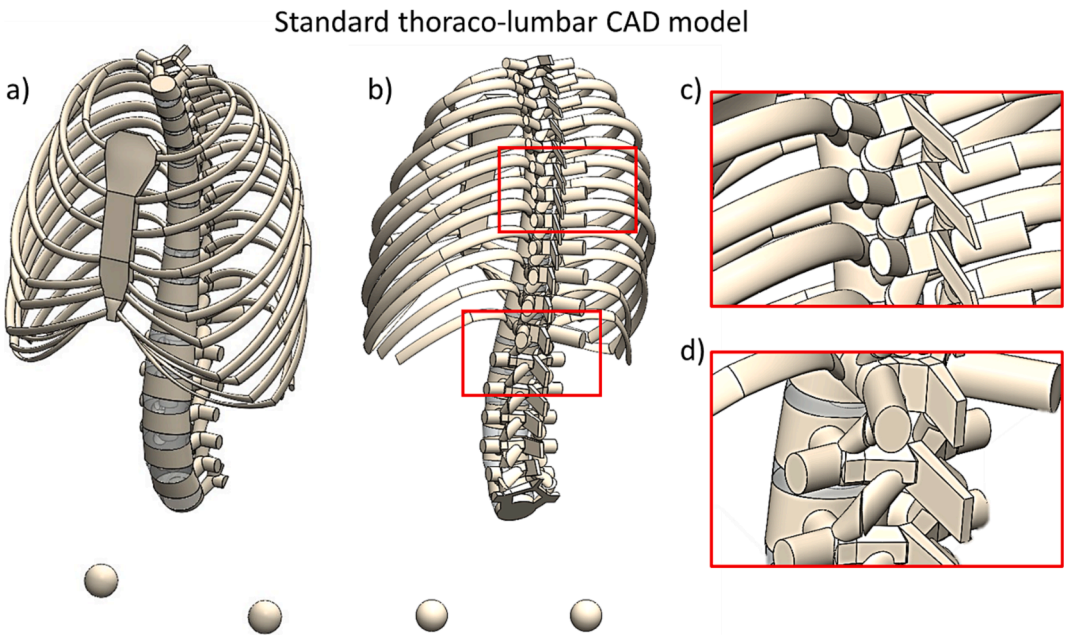

Fig. 1. Anterior (a) and posterior (b) views of the standard CAD model representative of a healthy male adult (age 46.3 years, height 167.8 cm, weight 67.8 kg) generated assuming average values for each independent parameter. Additional views (c, d) show detail of VA, spinal processes, FJs and the costo-vertebral junction (for the sake of clarity ligaments are not displayed).

anisotropic Holzapfel-Gasser-Ogden formulation (five parameters: C_{10}, D, k_1, k_2, k) was used for the AF (Eberlein et al., 2011; Gasser et al., 2006). A local reference system was assumed for each IVD, having a radial axis pointing outward the NP, a caudo-cranial axis pointing upward, and a coherent orthogonal circumferential axis; two families of fibers were inclined of ± 33.8° with respect to the horizontal plane (Eberlein et al., 2011). First-order hyperelastic isotropic Ogden formulation (three parameters: μ, α, D) was used for all ligaments (Martins et al., 2006; Bint-E-Siddiq, 2019) (Supplementary Material–Tables 2, 3).

L4-L5 FSU FEM: a backward stepwise calibration approach ensured adequate material property assignment to the lumbar AFs divided in quadrants, seven spinal ligaments (namely: ALL, PLL, FL, CL, ISL, SSL, ITL), and FJs. Constitutive parameters were iteratively changed until the range of motions (RoMs) predicted under pure moments of ± 1, ±2.5, ±5, ±7.5, ±10 Nm in flexion–extension, lateral bending and axial torsion fell within 1 SD (standard deviation, as a measure of dispersion) of the *in vitro* measurements (Heuer et al., 2007). We assumed uniform mechanical properties across the thoraco-lumbo-sacral segment (T12-S1).

T2-T3, T6-T7, T10-T11 FSUs FEMs: a backward stepwise calibration approach ensured adequate material property assignment to the thoracic AFs, seven spinal ligaments, and the FJs based on *in vitro* RoMs measured under pure moments of ± 1, ±2.5 Nm (Wilke et al., 2020) applied on the entire thoracic segment. We assumed uniform mechanical properties across the thoracic segment (T1-T12).

T1-T2-R2, T5-T6-R6, T9-T0-R10 FEMs: a backward stepwise calibration approach ensured adequate material property assignment to the costo-vertebral ligaments (namely RL, ICTL, LCTL, SCTL) based on *in vitro* RoMs measure at ± 0.6 Nm in torsion, caudal/cranial and ventral/dorsal flexion (Lemosse et al., 1998). We assumed uniform mechanical properties across three thoracic regions (T1-T4 + R1-R4, T5-T8 + R5-R8, and T9-T12 + R9-R12).

2.4. Case study: Validation of the thoraco-lumbo-sacral FEM

The remaining lumbar parts were imported and meshed to generate a standard thoraco-lumbo-sacral (T12-S1) FEM (Supplementary Material–Tables 2). We assessed the L1-S1 FEM by comparing the RoMs under pure moments of ± 7.5 Nm (±5 Nm in axial torsion) with *in vitro* data (Wang et al., 2022, La Barbera et al., 2018), as well as comparing both RoMs and intradiscal pressure (IDP) under complex loadings (Follower Loads + Moment) with *in silico* data by 8 FEMs (Dreischarf et al., 2014), *in vitro* (Brinckmann and Grootenboer, 1991), and *in vivo* data (Wilke et al., 2001). As for the T12-L1 FSU, only the RoM was compared with *in vitro* data under pure moments ± 5 Nm (Oxland et al., 1992, Couvertier et al., 2017).

2.5. Case study: Validation of the thoracic FEM with/without rib cage

The remaining thoracic parts were imported and meshed to generate a standard T1-T12 FEM (Supplementary Material–Tables 3). We assessed the thoracic FEM with/without the ribcage by comparing the RoMs under pure moments of ± 2Nm with *in vitro* data (Liebsch et al., 2017).

3. Results

3.1. Parametric thoraco-lumbar spine CAD model generator

Regression analyses: Supplementary Material–Tables 1 collects the best-fitted regression coefficients for each dependent parameters and the goodness-of-fit for each generated analytical equation. Overall, the anterior and posterior columns' dependent parameters were predicted within 0.6 mm and 1.5°; ribcage and sternum parameters were predicted within 0.7 mm and 0.6°. R^2 and RMSE were generally satisfactory (Supplementary Material–Table 1).

Standard CAD model: Fig. 1 collects different views of the generated standard CAD model, with detail of VA, spinal processes, FJs and the costo-vertebral junction.

Assessment and validation: the global sagittal alignment parameters of the standard CAD model compared well with *in vivo* published data (Fig. 2.a). Ribs' chord and arc lengths, as well as sternum position and orientation relative to the thoracic spine, were always within 1 SD of the *ex vivo* measurements (Fig. 2.b).

a) Sagittal spinal alignment

Parameter	Standard CAD model	*in vivo* cohorts Avg±SD [min; max]			
		Harrison et al. 2001 (n=30, 28±6.6y.)	Pesenti et al. 2018 (n=119, 50.7±17y.)	Vrtovec et al. 2023 (n=330, 45.3±18.1y.)	Fasser et al. 2021 (n=145,)
TK (°)	45	45.6±15.4			33.1±11.4 [5.5; 63.6]
LL(°)	58		58.1±13 [10; 89]		50.3±13.7 [0.8; 83.2]
SS (°)	38		38±8.8 [13.8; 65.4]		34.4±10.2 [10; 64]
PI (°)	45.9		52±11.4 [25; 84.7]	45.9±7.4	
PTH (mm)	104.9			104.9±8.6	

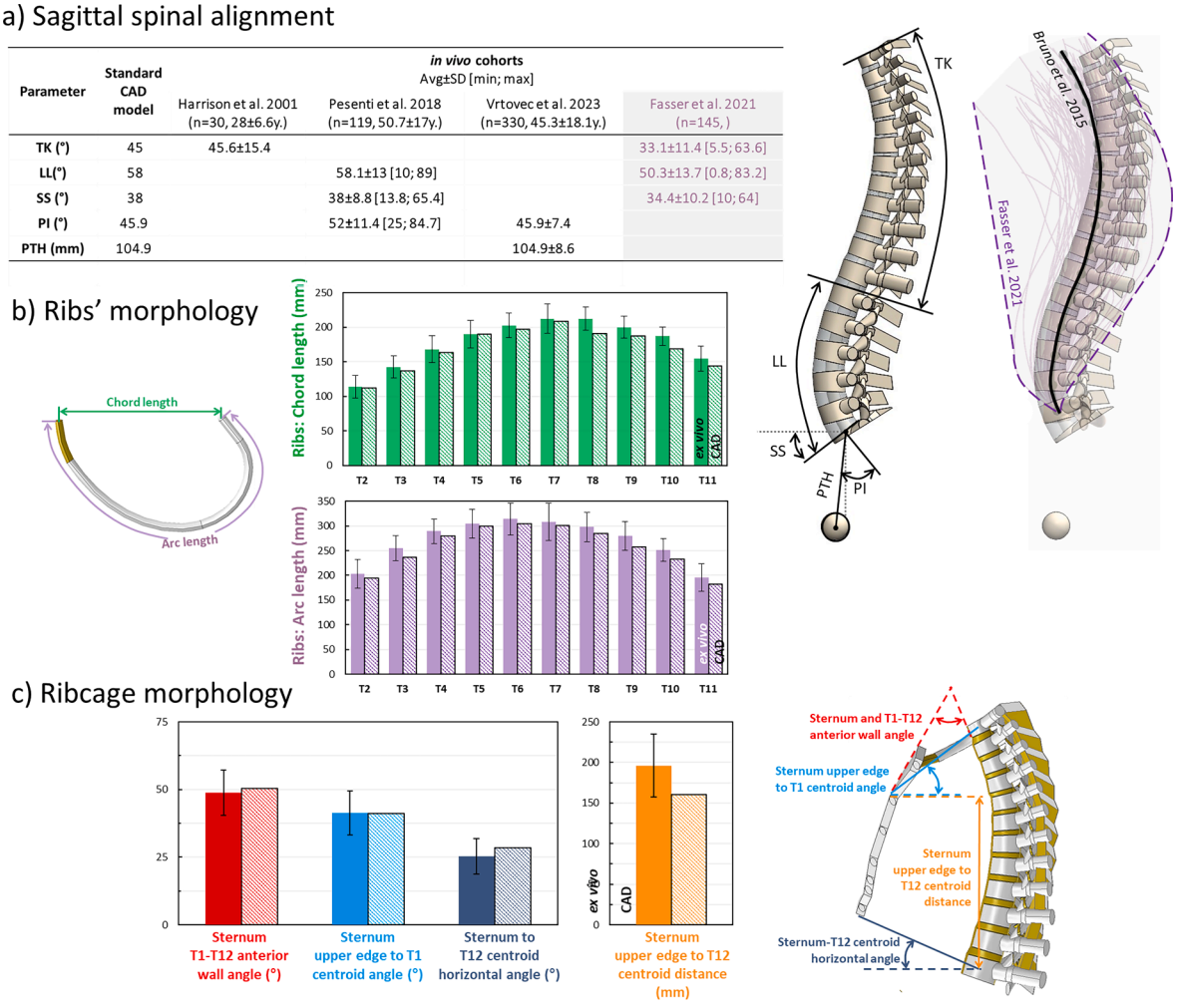

Fig. 2. a) quantitative and qualitative comparison of the sagittal alignment parameters assumed to generate the standard cad model of a healthy male adult (age 46.3 years, height 167.8 cm, weight 67.8 kg) with the measurements collected *in vivo* (Vrtovec et al., 2023, Vrtovec et al., 2012, Pesenti et al., 2018, Harrison et al., 2001, Fasser et al., 2021, Bruno et al., 2015). b) Ribs' chord and arc lengths assessed on the standard CAD model by comparison with *ex vivo* measurements (Dansereau and Stokes, 1988). c) Resulting sternum position and orientation relative to the thoracic segment assessed on the standard CAD model by comparison with *in vivo* data (Burgos et al., 2021).

3.2. Case study: Calibration of lumbar and thoracic FSUs

L4-L5 FSU: the calibrated constitutive parameters for IVD, spinal ligaments and FJs resulted in satisfactory agreement with *in vitro* experiments under pure moments (Heuer et al., 2007) (Fig. 3, Supplementary Material–Fig. 1).

T2-T3, T6-T7, T10-T11 FSUs: the calibrated constitutive parameters for IVDs, spinal ligaments and FJs resulted in satisfactory agreement with *in vitro* data under pure moments (Wilke et al., 2020) (Fig. 4).

T1-T2-R2, T5-T6-R6, T9-T0-R10: the calibrated constitutive parameters for costal ligaments resulted generally in satisfactory agreement with *in vitro* data (Lemosse et al., 1998), although a more flexible data was predicted in torsion and ventral-dorsal flexion for distal FSU (Fig. 5.a,b,c).

3.3. Case study: Validation of the thoraco-lumbo-sacral FEM

The assessment of the T12-S1 FEM proved accurate in predicting local RoMs (Fig. 6.a) and global RoMs (Fig. 6.b) under pure moments by comparison with *in vitro* measurements (Wang et al., 2022, La Barbera et al., 2018, Couvertier et al., 2017, Oxland et al., 1992), also providing results in agreement with *in silico* data predicted using other lumbar FEMs (Dreischarf et al., 2014).

The IDP predicted on L4-L5 proved to be sensitive to simple axial compressive loads (Fig. 6.c), being consistent with other FEM (Dreischarf et al., 2014) and well within *in vitro* measurements (Brinckmann and Grootenboer, 1991); even applying complex loadings, the lumbar FEM could predict IDPs at multiple levels in good agreement with published FEMs (Dreischarf et al., 2014) and *in vivo* measures (Wilke et al., 2001) (Fig. 6.d). Our model could appreciate the increased stability provided by the follower load and a slight increasing trend when moving from cranial to caudal FSU.

3.4. Case study: Validation of the thoracic FEM with/without rib cage

The T1-T12 FEM predicted RoMs under pure moments was comparable with *in vitro* data (Liebsch et al., 2017), being generally within 1 SD (Fig. 7); the thoracic FEM could also appreciate the stiffening effect of the ribcage in lateral bending and axial rotation, being less sensitive in flexion–extension.

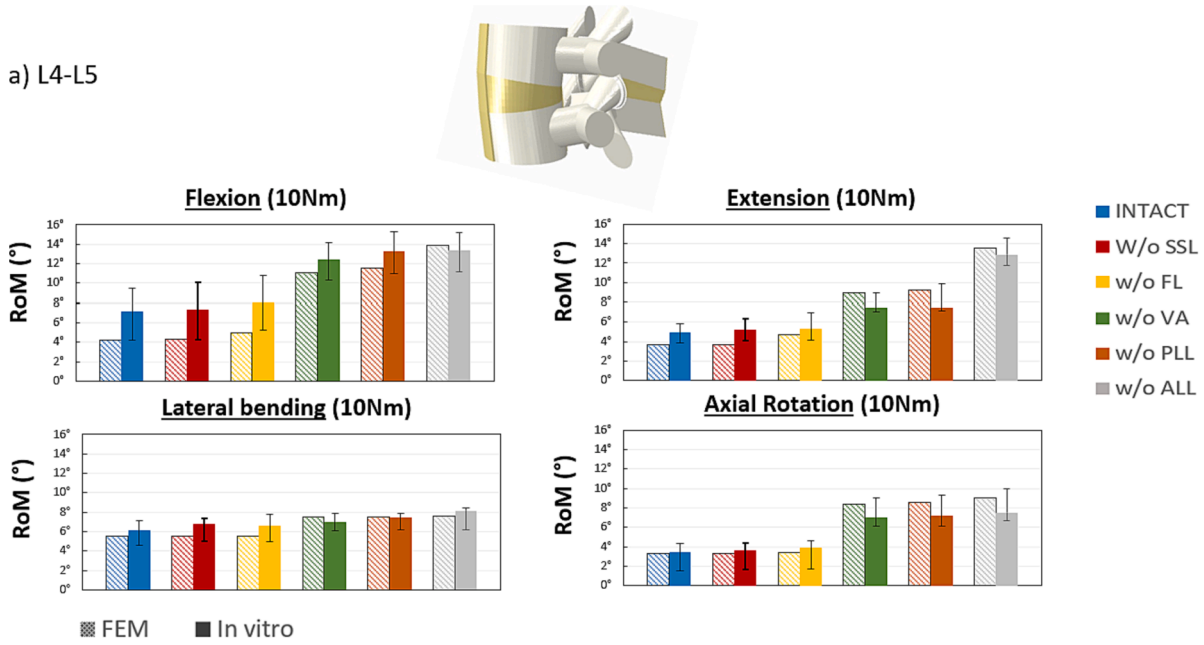

Fig. 3. Comparison of the RoM predicted using L4-L5 FSU FEM model after calibration vs. *in vitro* measurements at ± 10Nm (Heuer et al., 2007).

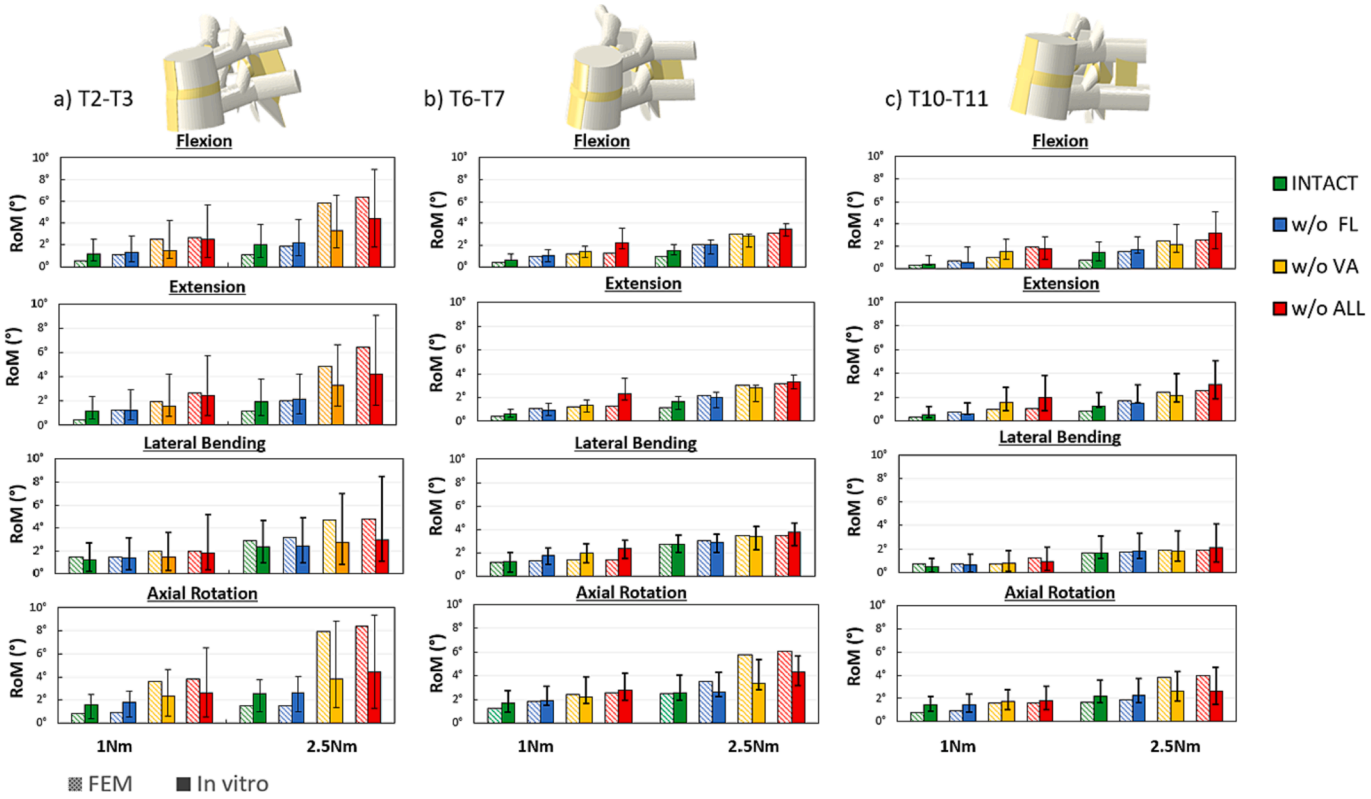

Fig. 4. Comparison of the RoM predicted using thoracic FSUs FEMs after calibration vs. *in vitro* measurements at ± 1 and ± 2.5 Nm vs. *in vitro* data (Wilke et al., 2020).

4. Discussion

4.1. Parametric thoraco-lumbar spine CAD model generator

A user-friendly parametric CAD model comprehensive of the thoraco-lumbar spine including the ribcage was herein developed. The proposed CAD model provides a general description of the spinal anatomy based on simplified features, which resulted to be accurate in describing vertebral and ribcage morphology (Figs. 1 and 2).

The automatic generation of any new spinal CAD model only requires eighteen independent parameters as input (one VBHP for each vertebra from T1 to S1), plus four global sagittal alignment parameters (PI, SS, LL, TK). This tool allows the automatic calculation of fifty-six dependent parameters, implemented as equations directly in the CAD

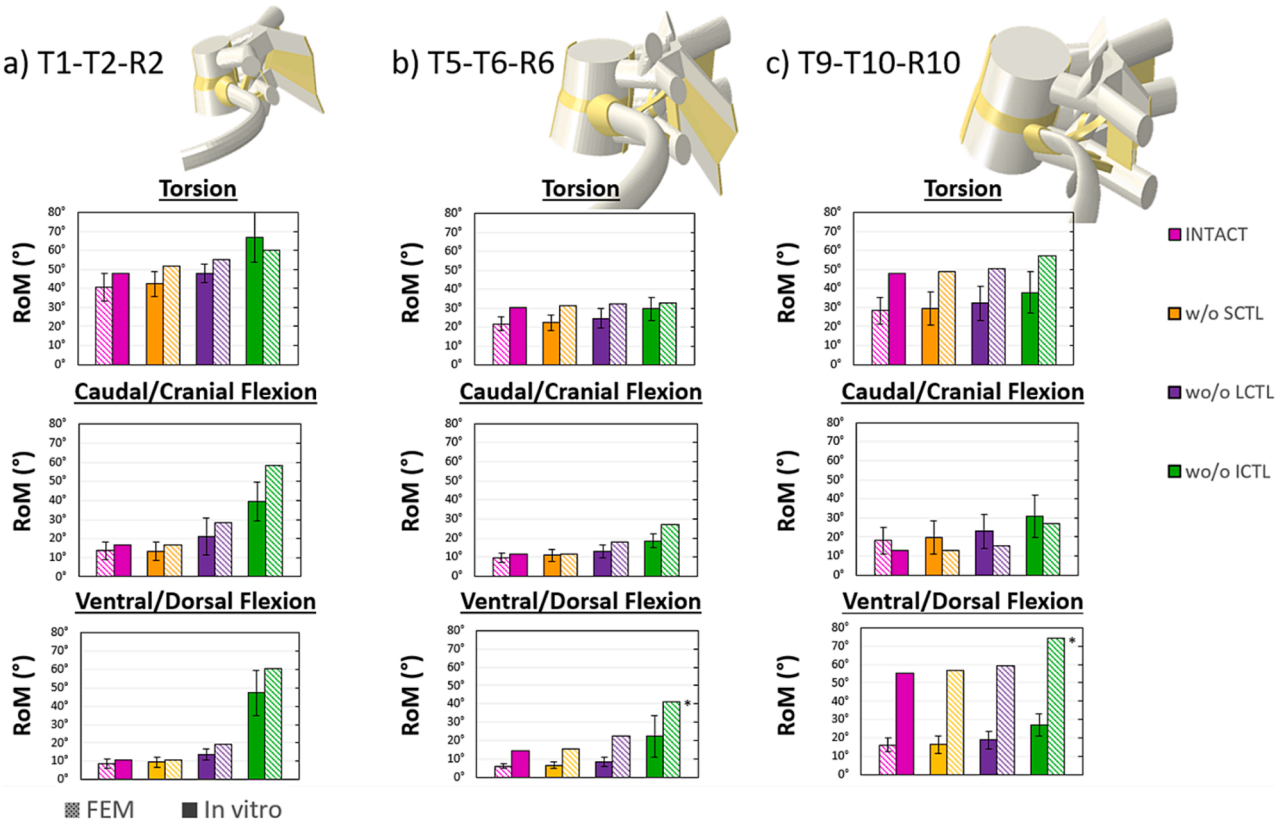

Fig. 5. Comparison of the RoM predicted using thoracic FSUs FEMs including the left rib after calibration vs. *in vitro* measurements at ± 0.6 Nm (Lemosse et al., 1998). '*' denotes simulations which did not achieve convergence, so they only provide an underestimation.

software and the update of the spine CAD model within few seconds. The proposed approach allows the generation of both arbitrary and patient-specific spine CAD models, as these few parameters can be easily measured on common clinical images. Whenever any input data is missing, the user could consider running a sensitivity analysis to study the effect of the unknown input parameters, or rely on the equations already implemented and based on average literature measurements (Supplementary Material–Tables 1). Whenever needed to investigate specific aspect not yet included in the presented CAD model, the user could anyway flexibly update the equations or modify them as needed. Of course, the user should always consider that the implemented equations rely on the experimental data used to build them, therefore, they may lose their significance when applied in a way different range of values. Moreover, as the CAD model is obtained as a complex assembly of different geometrical parts and specific constraints in terms of relative position and orientation have been implemented to ensure their correct positioning, the user may experience a regeneration failure. In this case, it may be necessary to perform some troubleshooting, identifying the source of error.

4.2. Case study: Calibration of lumbar and thoracic FSUs

The parametric CAD model was successfully used to generate standard FEMs of isolated lumbar FSU and three thoracic FSUs for the proximal, medial and distal segments, often regarded as homogenous in current *in silico* spine models (La Barbera et al., 2021a,b). This step was necessary in order to calibrate the mechanical properties of the soft tissues, in particular the IVDs, the spinal and costo-vertebral ligaments based on established *in vitro* measurements (Heuer et al., 2007, Wilke et al., 2020, Lemosse et al., 1998), ensuring an accurate description of the increased stability provided by the passive osteo-ligamentous structures sequentially added to the model.

4.3. Case study: Validation of the thoraco-lumbo-sacral FEM

The assessment of the T12-S1 FEM demonstrated that the material properties calibrated on L4-L5 could be extended to the entire thoraco-lumbar spine model, as kinematics (i.e. RoMs) and dynamics (i.e. IDP) could be accurately predicted both applying bending moments alone and in combination with follower load. Predictions nicely agreed both with *in vitro* (Wang et al., 2022, La Barbera et al., 2018, Couvertier et al., 2017, Oxland et al., 1992, Brinckmann and Grootenboer, 1991), *in vivo* (Wilke et al., 2001) measurements and were totally comparable with other published lumbar FEM (Dreischarf et al., 2014), with particular detail on the stabilizing effect of the follower load especially for more caudal FSUs.

4.4. Case study: Validation of the thoracic FEM with/without rib cage

The assessment of the thoracic T1-T12 FEM proved that the material properties calibrated on the three thoracic FSUs could be generally extended to the proximal, medial and distal thoracic segments, despite the model was more flexible in torsion and ventral-dorsal flexion for distal FSU. Such finding should be related with the simplification in describing the costo-vertebral ligaments without relying on sufficient information about their features and mechanical properties. Nevertheless, our models could appreciate the increased stability provided by the ribcage especially in lateral bending and axial torsion (Liebsch et al., 2017).

4.5. Advantages, limitations and future steps

The main advantage of the proposed parametric CAD model relies in its simplicity, as only 22 inputs (18 VBHPs + 4 sagittal balance parameters, namely PI, SS, LL, and TK) are required to automatically

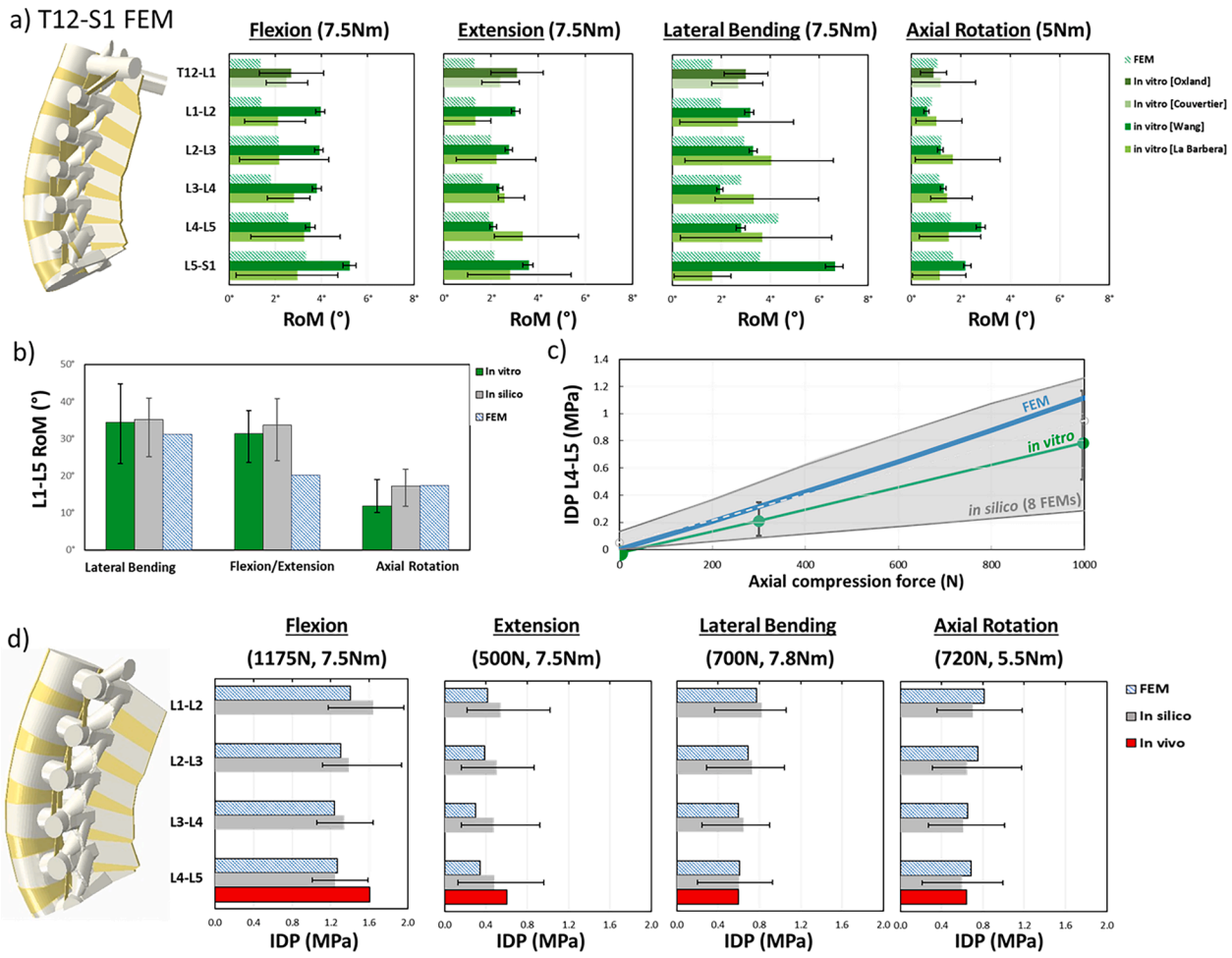

Fig. 6. a) assessment of local RoM predicted for each FSU using T12-S1 FEM vs. *in vitro* measurements under pure moments vs. *in vitro* data at ± 7.5 (Wang et al., 2022, La Barbera et al., 2018) or ± 5 Nm (Couvertier et al., 2017, Oxland et al., 1992).b) Assessment of global RoM predicted using L1-S1 FEM vs. *in vitro* measurements at ± 7.5 Nm vs. *in vitro* data (Wang et al., 2022) and *in silico* data by 8 FEMs (Dreischarf et al., 2014).c) Assessment of IDP predicted as a function of follower load using L1-S1 FEM vs. *in silico* data by 8 FEMs (Dreischarf et al., 2014) vs. *in vitro* measurements at 0, 300 and 1000 N (Brinckmann and Grootenboer, 1991). d) Assessment of IDP predicted on lumbar disks using L1-S1 FEM vs. *in silico* data by 8 FEMs under complex loadings (Dreischarf et al., 2014) vs. *in vivo* measurements on L4-L5 (Wilke et al., 2001).

generate any new spine model comprehensive of the thoraco-lumbar spine and the ribcage. To the best of our knowledge this is the simplest fully-parametric spine model up-to-date available including an articulated ribcage. For the sake of comparison, Niemeyer et al. and Bashkuev et al. proposed two similar model generators requiring seventeen parameters for each vertebra plus additional six for each intervertebral region and spinal processes (Niemeyer et al., 2012, Bashkuev et al., 2018); therefore, their approach required a total of 40 inputs to generate only a L4-L5 FSU. Lavaste et al., (1992) required six inputs parameters per each vertebra, to be identified on antero-posterior and lateral X-ray images; therefore, a total of 36 inputs are needed to generate an entire lumbo-sacral segment. Nikkhoo et al. (Nikkhoo et al., 2020) recently proposed a parametric lumbar spine model based on 21 parameters for each vertebra.

One independent parameter per vertebra (against 6 for Lavaste et al., (1992), 21 for Nikkhoo et al., (2020) and 40 for both Bashkuev et al., (2018), Niemeyer et al., (2012)) implies having one unique parameter to scale the vertebral morphology, which may be considered a limitation when there are consistent deviations from the geometrical design parametrically implemented in the CAD model. Of course, depending on the research question to be answered, a trade-off between an accurate description of spinal morphology and the number of input parameters to be controlled should be always considered. Whenever required, the user may consider removing some simplification and increasing the number of independent parameters to be defined as inputs.

Spinal morphology was reduced to simplified features, perfectly symmetrical with respect to the sagittal plane. The developed spine CAD model proved consistent in describing the average vertebral and ribcage morphologies of a healthy adult in the physiological range. Therefore, applications of the proposed CAD model to represent unphysiological or pathological conditions involving large spinal deviations from the sagittal plane, as often met in scoliotic patients presenting with coronal and transverse plane deformities, should be carefully considered and avoided. It is worth mentioning that the parametric CAD model could be anyway used to describe the variety of different sagittal morphotypes met in the normal population, as described according to Roussouly's classification (Roussouly et al., 2005; Laouissat et al., 2018). This is the main reason why we have explicitly implemented PI, SS, LL and TK as independent parameters. Considered the trigonometric redundancy existing between specific sagittal balance parameters, different independent parameter may be adopted (i.e. PT, pelvic tilt) and the corresponding equation (PT = PI – SS) implemented in the parametric CAD model.

Calibration of the soft tissues and assessment were performed under established loading conditions, either including pure bending moments or combined with follower load. We only considered passive osteo-

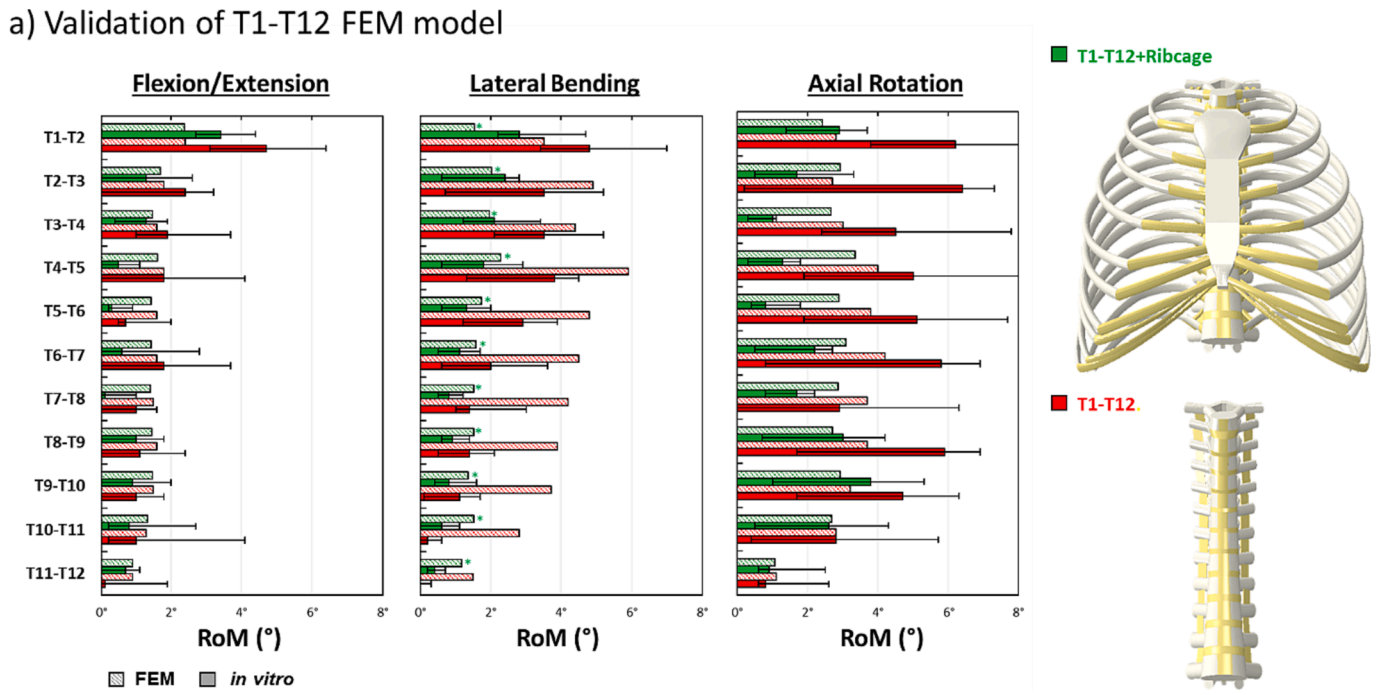

Fig. 7. Comparison of the local RoM predicted for each FSU using T1-T12 FEM with/without ribcage vs. *in vitro* measurements at ± 2Nm vs. *in vitro* data (Liebsch et al., 2017).

ligamentous structures, neglecting the active role of muscles which are certainly involved in loadings *in vivo*. Next steps could, therefore, parametrize and integrate active structures (i.e. muscles, abdomen, …) (Anderson et al., 2012, Ghezelbash et al., 2016), allowing to investigate more realistic motor tasks and challenging clinical applications.

Uniform mechanical properties were assumed across the upper-thoracic, middle-thoracic, lower-thoracic, as well as the thoraco-lumbo-sacral segments, as calibrated on specific FSU. Moreover, similar general criteria were assumed to split the IVD into NP and AF, and to draw the spinal and costo-vertebral ligaments for each FSU. Although this may not accurately represent the expected continuous variations in terms of mechanical properties and morphometrical featuresof every single osteo-ligamentous tissue, the results herein reported supports the feasibility of our parametric CAD model to generate credible FEMs either for the thoraco-lumbo-sacral spine and the thoracic spine with or without the articulated ribcage.

Next steps could move towards the parametrization of geometrical parameters also for the spinal ligaments, implementing, for instance, variations in terms of thickness and cross-sections, beside assuming anisotropic hyperelastic constitutive laws (Hortin et al., 2015, Robertson et al., 2013). Given the complexity of the costo-vertebral joint and the lack of detailed information about thoracic ligaments, it is important to notice that we aimed at creating a reasonable, yet simple geometry for most osteo-ligamentous structures. Therefore, some aspect could be surely improved as far as more data will be collected. Overall, the calibration and validation steps demonstrated the feasibility of generating a standard FEM representing a healthy male spine providing relevant insights about thoraco-lumbar spine biomechanics and paved the way towards clinically relevant applications.

CRediT authorship contribution statement

Emilia Bellina: Data curation, Formal analysis, Methodology, Software, Visualization, Writing – original draft, Writing – review & editing. **Maria Elvira Laurino:** Data curation, Formal analysis, Methodology, Software, Writing – review & editing. **Alice Perego:** Data curation, Formal analysis, Methodology, Software, Writing – review & editing. **Alice Pezzinga:** Data curation, Formal analysis, Methodology, Software, Writing – review & editing. **Linda Carpenedo:** Data curation, Formal analysis, Methodology, Writing – review & editing. **Davide Ninarello:** Data curation, Formal analysis, Methodology, Writing – review & editing. **Luigi La Barbera:** Conceptualization, Funding acquisition, Investigation, Methodology, Project administration, Resources, Software, Supervision, Validation, Visualization, Writing – original draft, Writing – review & editing.

Declaration of competing interest

The authors declare that they have no known competing financial interests or personal relationships that could have appeared to influence the work reported in this paper.

Acknowledgements

This work was partially funded by MIUR FISR—FISR2019_03221 CECOMES.

Appendix A. Supplementary material

Supplementary data to this article can be found online at https://doi.org/10.1016/j.jbiomech.2024.111951.

References

Abuzayed, B., Tutunculer, B., Kucukyuruk, B., Tuzgen, S., 2010. Anatomic basis of anterior and posterior instrumentation of the spine: morphometric study. Surg. Radiol. Anat. 32 (1), 75–85. https://doi.org/10.1007/s00276-009-0545-4.

Anderson, D.E., D'Agostino, J.M., Bruno, A.G., Manoharan, R.K., Bouxsein, M.L., 2012. Regressions for estimating muscle parameters in the thoracic and lumbar trunk for use in musculoskeletal modeling. J Biomech 3;45 (1), 66–75. https://doi.org/10.1016/j.jbiomech.2011.10.004.

Bashkuev, M., Reitmaier, S., Schmidt, H., 2018. Effect of disc degeneration on the mechanical behavior of the human lumbar spine: a probabilistic finite element study. Spine J. 18 (10), 1910–1920. https://doi.org/10.1016/j.spinee.2018.05.046.

Bassani, T., Ottardi, C., Costa, F., Brayda-Bruno, M., Wilke, H.J., Galbusera, F., 2017. Semiautomated 3D spine reconstruction from biplanar radiographic images:

Prediction of intervertebral loading in scoliotic subjects. Front. Bioeng. Biotechnol. 20 (5), 1. https://doi.org/10.3389/fbioe.2017.00001.
Bint-E-Siddiq, A., 2019. Mechanical characterisation and computational modelling of spinal ligaments. Ph.D. Thesis. University of Leeds.
Brinckmann, P., Grootenboer, H., 1991. Change of disc height, radial disc bulge, and intradiscal pressure from discectomy. An in vitro investigation on human lumbar discs. Spine 16, 641–646.
Bruno, A.G., Bouxsein, M.L., Anderson, D.E., 2015. Development and validation of a musculoskeletal model of the fully articulated thoracolumbar spine and rib cage. J. Biomech. Eng. 137 (8), 081003 https://doi.org/10.1115/1.4030408.
Burgos, J., Barrios, C., Mariscal, G., Lorente, A., Lorente, R., 2021. Non-uniform segmental range of motion of the thoracic spine during maximal inspiration and exhalation in healthy subjects. Front. Med. (Lausanne) 30 (8), 699357. https://doi.org/10.3389/fmed.2021.699357.
Couvertier, M., Germaneau, A., Saget, M., Doumalin, J.C., Dupré, P., Brémand, F., Hesser, F., Brèque, C., Roulaud, M., Monlezun, O., Vendeuvre, T., Rigoard, P., 2017. Biomechanical analysis of the thoracolumbar spine under physiological loadings: Experimental motion data corridors for validation of finite element models. Proc. Inst. Mech. Eng. H. 231 (10), 975–981. https://doi.org/10.1177/0954411917719740.
Cui, X.G., Cai, J.F., Sun, J.M., Jiang, Z.S., 2015. Morphology study of thoracic transverse processes and its significance in pedicle-rib unit screw fixation. J. Spinal Disord. Tech. 28, E74–E77.
Dansereau, J., Stokes, I.A., 1988. Measurements of the three-dimensional shape of the rib cage. J Biomech. 21 (11), 893–901. https://doi.org/10.1016/0021-9290(88)90127-3.
Dreischarf, M., Zander, T., Shirazi-Adl, A., Puttlitz, C.M., Adam, C.J., Chen, C.S., Goel, V. K., Kimm, A., Kiapourm, Y.H., Labus, K.M., Little, J.P., Park, W.M., Wang, Y.H., Wilke, H.J., Rohlmann, A., Schmidt, H., 2014. Comparison of eight published static finite element models of the intact lumbar spine: predictive power of models improves when combined together. J. Biomech. 47 (8), 1757–1766. https://doi.org/10.1016/j.jbiomech.2014.04.002.
Eberlein, R., Holzapfel, G.A., Schulze-Bauer, C.A.J., 2011. An anisotropic model for annulus tissue and enhanced finite element analyses of intact lumbar disc bodies. Comput. Methods Biomech. Biomed. Engin. 4, 209–229. https://doi.org/10.1080/10255840108908005.
El Bojairami, I., El-Monajjed, K., Driscoll, M., 2020. Development and validation of a timely and representative finite element human spine model for biomechanical simulations. Sci. Rep. 10, 21519. https://doi.org/10.1038/s41598-020-77469-1.
Fasser, M.R., Jokeit, M., Kalthoff, M.G., Romero, D.A., Trache, T., Snedeker, J.G., Farshad, M., Widmer, J., 2021. Subject-specific alignment and mass distribution in musculoskeletal models of the lumbar spine. Front. Bioeng. Biotechnol. 31 (9), 721042 https://doi.org/10.3389/fbioe.2021.721042.
Gasser, T.C., Ogden, R.W., Holzapfel, G.A., 2006. Hyperelastic modelling of arterial layers with distributed collagen fibre orientations. J. R. Soc. Interface 3 (6), 15–35. https://doi.org/10.1098/rsif.2005.0073.
Ghezelbash, F., Shirazi-Adl, A., Arjmand, N., El-Ouaaid, Z., Plamondon, A., Meakin, J.R., 2016. Effects of sex, age, body height and body weight on spinal loads: Sensitivity analyses in a subject-specific trunk musculoskeletal model. J. Biomech. 3;49 (14), 3492–3501. https://doi.org/10.1016/j.jbiomech.2016.09.026.
Harrison, D.E., Harrison, D.D., Cailliet, R., Troyanovich, S.J., Janik, T.J., Holland, B., 2001. Radiographic analysis of lumbar lordosis: centroid, Cobb, TRALL, and Harrison posterior tangent methods. Spine (Phila Pa 1976) 1;26 (11), E235–E242. https://doi.org/10.1097/00007632-200106010-00003.
Heuer, F., Schmidt, H., Klezl, Z., Claes, L., Wilke, H.J., 2007. Stepwise reduction of functional spinal structures increase range of motion and change lordosis angle. J. Biomech. 40 (2), 271–280. https://doi.org/10.1016/j.jbiomech.2006.01.007.
Holcombe, S.A., Wang, S.C., Grotberg, J.B., 2016. Modeling female and male rib geometry with logarithmic spirals. J. Biomech. 49 (13), 2995–3003. https://doi.org/10.1016/j.jbiomech.2016.07.021.
Holcombe, S.A., Wang, S.C., Grotberg, J.B., 2017. The effect of age and demographics on rib shape. J. Anat. 231 (2), 229–247. https://doi.org/10.1111/joa.12632.
Hortin, M., Graham, S., Boatwright, K., Hyoung, P., Bowden, P., 2015. Transversely isotropic material characterization of the human anterior longitudinal ligament. J. Mech. Behav. Biomed. Mater. 45, 75–82. https://doi.org/10.1016/j.jmbbm.2015.01.020.
Ignasiak, D., Dendorfer, S., Ferguson, S.J., 2016. Thoracolumbar spine model with articulated ribcage for the prediction of dynamic spinal loading. J. Biomech. 11;49 (6), 959–966. https://doi.org/10.1016/j.jbiomech.2015.10.010.
Kapandji, I., 2012. Fisiología Articular Tomo 3. Tronco y raquis, Editorial Médica Panamericana S.A.
Kaur, K., Singh, R., Prasath, V., Magu, S., Tanwar, M., 2016. Computed tomographic-based morphometric study of thoracic spine and its relevance to anaesthetic and spinal surgical procedures. J. Clin. Orthop. Trauma 7 (2), 101–108. https://doi.org/10.1016/j.jcot.2015.12.002.
Kunkel, M.E., Herkommer, A., Reinehr, M., Böckers, T.M., Wilke, H.J., 2011. Morphometric analysis of the relationships between intervertebral disc and vertebral body heights: an anatomical and radiographic study of the human thoracic spine. J. Anat. 219 (3), 375–387. https://doi.org/10.1111/j.1469-7580.2011.01397.x.
La Barbera, L., Brayda-Bruno, M., Liebsch, C., Villa, T., Luca, A., Galbusera, F., Wilke, H. J., 2018. Biomechanical advantages of supplemental accessory and satellite rods with and without interbody cages implantation for the stabilization of pedicle subtraction osteotomy. Eur. Spine J. 27 (9), 2357–2366. https://doi.org/10.1007/s00586-018-5623-z.
La Barbera, L., Larson, A.N., Aubin, C.E., 2021. How do spine instrumentation parameters influence the 3D correction of thoracic adolescent idiopathic scoliosis? A patient-specific biomechanical study. Clin. Biomech. (Bristol, Avon) 84, 105346. https://doi.org/10.1016/j.clinbiomech.2021.105346.
La Barbera, L., Larson, A.N., Rawlinson, J., Aubin, C.E., 2021. In silico patient-specific optimization of correction strategies for thoracic adolescent idiopathic scoliosis. Clin. Biomech. (Bristol, Avon) 81, 105200. https://doi.org/10.1016/j.clinbiomech.2020.105200.
Laouissat, F., Sebaaly, A., Gehrchen, M., Roussouly, P., 2018. Classification of normal sagittal spine alignment: refounding the Roussouly classification. Eur. Spine J. 27 (8), 2002–2011. https://doi.org/10.1007/s00586-017-5111-x.
Lavaste, F., Skalli, W., Robin, S., Roy-Camille, R., Mazel, C., 1992. Three-dimensional geometrical and mechanical modelling of the lumbar spine. J. Biomech. 25 (10), 1153–1164. https://doi.org/10.1016/0021-9290(92)90071-8.
Lavecchia, C.E., Espino, D.M., Moerman, K.M., Tse, K.M., Robinson, D., Lee, P.V.S., Shepherd, D.E.T., 2018. Lumbar model generator: a tool for the automated generation of a parametric scalable model of the lumbar spine. J. R. Soc. Interface 15 (138), 20170829.
Laville, A., Laporte, S., Skalli, W., 2009. Parametric and subject-specific finite element modelling of the lower cervical spine. Influence of geometrical parameters on the motion patterns. J. Biomech. 42 (10), 1409–1415. https://doi.org/10.1016/j.jbiomech.2009.04.007.
Lemosse, D.L., Rue, O., Diop, A., Skalli, W., Marec, P., Lavaste, F., 1998. Characterization of the mechanical behaviour parameters of the costo-vertebral joint. Eur. Spine J. 7 (1), 16–23. https://doi.org/10.1007/s005860050021.
Liebsch, C., Graf, N., Appelt, K., Wilke, H., 2017. The rib cage stabilizes the human thoracic spine: An in vitro study using stepwise reduction of rib cage structures. PLoS One 1;12 (6), e0178733. https://doi.org/10.1371/journal.pone.0178733.
Martins, P.N., Jorge, R.M., Ferreira, A., 2006. A comparative study of several material models for prediction of hyperelastic properties: Application to silicone-rubber and soft tissues. Strain 42 (3), 135–147.
Maurel, N., Lavaste, F., Skalli, W., 1997. A three-dimensional parameterized finite element model of the lower cervical spine. Study of the influence of the posterior articular facets. J. Biomech. 30 (9) https://doi.org/10.1016/S0021-9290(97)00056-0.
Mohr, M., Abrams, E., Engel, C., Long, W.B., Bottlang, M., 2007. Geometry of human ribs pertinent to orthopedic chest-wall reconstruction. J. Biomech. 40 (6), 1310–1317. https://doi.org/10.1016/j.jbiomech.2006.05.017.
Niemeyer, F., Wilke, H.J., Schmidt, H., 2012. Geometry strongly influences the response of numerical models of the lumbar spine - a probabilistic finite element analysis. J. Biomech. 45 (8), 1414–1423. https://doi.org/10.1016/j.jbiomech.2012.02.021.
Nikkhoo, M., Khoz, Z., Cheng, C.-H., Niu, C.-C., El-Rich, M., Khalaf, K., 2020. Development of a novel geometrically-parametric patient-specific finite element model to investigate the effects of the lumbar lordosis angle on fusion surgery. J. Biomech. https://doi.org/10.1016/j.jbiomech.2020.109722.
Ottardi, C.L., Barbera, L., Pietrogrande, L., Villa, T., 2016. Vertebroplasty and kyphoplasty for the treatment of thoracic fractures in osteoporotic patients: a finite element comparative analysis. J. Appl. Biomater. Funct. Mater. 14, e197–e204. https://doi.org/10.5301/jabfm.5000287.
Oxland, T.R., Lin, R.M., Panjabi, M.M., 1992. Three-Dimensional mechanical properties of the thoracolumbar junction. J. Orthop. Res. 10 (4) https://doi.org/10.1002/jor.1100100412.
Panjabi, M.M., Takata, K., Goel, V., Federico, D., Oxland, T., Duranceau, J., Krag, M., 1991. Thoracic human vertebrae. Quantitative three-dimensional anatomy. Spine (Phila Pa 1976) 16 (8), 888–901. https://doi.org/10.1097/00007632-199108000-00006.
Panjabi, M.M., Goel, V., Oxland, T., Takata, K., Duranceau, J., Krag, M., Price, M., 1992. Human lumbar vertebrae. Quantitative three-dimensional anatomy. Spine (Phila Pa 1976) 17 (3), 299–306. https://doi.org/10.1097/00007632-199203000-00010.
Panjabi, M.M., Oxland, T., Takata, K., Goel, V., Duranceau, J., Krag, M., 1993. Articular facets of the human spine. Quantitative three-dimensional anatomy. Spine (Phila Pa 1976) 18 (10), 1298–1310. https://doi.org/10.1097/00007632-199308000-00009.
Park, B.D., Ebert, S., Reed, M.P., 2017. A parametric model of child body shape in seated postures. Traffic. Inj. Prev. 4;18 (5), 533–536. https://doi.org/10.1080/15389588.2016.1269173.
Pesenti, S., Lafage, R., Stein, D., Elysee, J.C., Lenke, L.G., Schwab, F.J., Kim, H.J., Lafage, V., 2018. The amount of proximal lumbar lordosis is related to pelvic incidence. Clin. Orthop. Relat. Res. 476 (8), 1603–1611. https://doi.org/10.1097/CORR.0000000000000380.
Robertson, D., Willardson, R., Parajuli, D., Cannon, A., Bowden, A.E., 2013. The lumbar supraspinous ligament demonstrates increased material stiffness and strength on its ventral aspect. J. Mech. Behav. Biomed. Mater. 17, 34–43. https://doi.org/10.1016/j.jmbbm.2012.07.009.
Rohlmann, A., Zander, T., Rao, M., Bergmann, G., 2009. Realistic loading conditions for upper body bending. J. Biomech. 11;42 (7), 884–890. https://doi.org/10.1016/j.jbiomech.2009.01.017.
Roussouly, P., Gollogly, S., Berthonnaud, E., Dimnet, J., 2005. Classification of the normal variation in the sagittal alignment of the human lumbar spine and pelvis in the standing position. Spine. 1;30 (3), 346–353. https://doi.org/10.1097/01.brs.0000152379.54463.65.
Schmidt, H., Galbusera, F., Rohlmann, A., Zander, T., Wilke, H.J., 2012. Effect of multilevel lumbar disc arthroplasty on spine kinematics and facet joint loads in flexion and extension: a finite element analysis. Eur. Spine J. 21 Suppl 5(Suppl 5), S663–S674. https://doi.org/10.1007/s00586-010-1382-1.
Shaw, J.D., Shaw, D.L., Cooperman, D.R., Eubanks, J.D., Li, L., Kim, D.H., 2015. Characterization of lumbar spinous process morphology: a cadaveric study of 2,955 human lumbar vertebrae. Spine J. 1;15 (7), 1645–1652. https://doi.org/10.1016/j.spinee.2015.03.007.

Vrtovec, T., Janssen, M.M., Pernuš, F., Castelein, R.M., Viergever, M.A., 2012. Analysis of pelvic incidence from 3-dimensional images of a normal population. Spine (Phila Pa 1976) 15;37 (8), E479–E485. https://doi.org/10.1097/BRS.0b013e31823770af.

Vrtovec, T., Janssen, M.M., Likar, B., Castelein, R.M., Viergever, M.A., Pernuš, F., 2013. Evaluation of pelvic morphology in the sagittal plane. Spine J. 13 (11), 1500–1509. https://doi.org/10.1016/j.spinee.2013.06.034.

Wang, Y., Cao, L., Bai, Z., Reed, M.P., Rupp, J.D., Hoff, C.N., Hu, J., 2016. A parametric ribcage geometry model accounting for variations among the adult population. J. Biomech. 6;49 (13), 2791–2798. https://doi.org/10.1016/j.jbiomech.2016.06.020.

Wang, W., Kong, C., Pan, F., Wang, W., Wu, X., Pei, B., Lu, S., 2022. Influence of Sagittal Lumbopelvic Morphotypes on the Range of Motion of Human Lumbar Spine: An In Vitro Cadaveric Study. Bioengineering (Basel) 20;9 (5), 224. https://doi.org/10.3390/bioengineering9050224.

Wilke, H.J., Grundler, S., Ottardi, C., Mathew, C.E., Schlager, B., Liebsch, C., 2020. In vitro analysis of thoracic spinal motion segment flexibility during stepwise reduction of all functional structures. Eur. Spine J. 29 (1), 179–185. https://doi.org/10.1007/s00586-019-06196-7.

Wilke, H., Neef, P., Hinz, B., Seidel, H., Claes, L., 2001. Intradiscal pressure together with anthropometric data–a data set for the validation of models. Clin. Biomech. (Bristol, Avon) 16 (Suppl 1), S111–S126. https://doi.org/10.1016/s0268-0033(00)00103-0.

Xiu, P., Shui, D., Wang, Q., Wang, G., Lan, Y., 2012. Anatomic and morphometric analysis of manubrium sterni as a source of autograft for anterior cervical fusion surgery using quantitative 3-dimensional computed tomographic scans. Spine 37. https://doi.org/10.1097/BRS.0b013e318252d27f. ISSN 03622436.